Scripta Materialia 252 (2024) 116276

Contents lists available at ScienceDirect

Scripta Materialia

journal homepage: www.journals.elsevier.com/scripta-materialia

Relating defect concentrations to spatially fluctuating lattice strains

Andrew R. Warwick *, Luca Reali, Sergei L. Dudarev

UK Atomic Energy Authority, Culham Science Centre, Abingdon, OX14 3DB, UK

ARTICLE INFO

MSC:
0000
1111

Keywords:
Materials characterisation
Residual stress
Eigenstrain
Lattice strain
Vacancy concentration

ABSTRACT

Measurements of lattice strain at high spatial resolution are becoming accessible and routine, owing to advances in imaging techniques such as 4D Scanning Transmission Electron Microscopy. This has the potential to enhance materials characterisation, but the data are difficult to interpret. We present a procedure for extracting local concentrations of isotropic defects, such as vacancies, from a spatially fluctuating strain field. The local dilatation is related to the defect concentration at *the same* point; strain fluctuations are directly proportional to concentration fluctuations by a factor determined by the Poisson ratio of the material. The inversion of strains to isotropic defect concentrations is demonstrated in molecular dynamics and finite element simulations of vacancy distributions in bcc W and fcc Au.

Many material properties are sensitive to their structural defects: high densities of dislocations lead to hardening, and diffusional creep is mediated by vacancies. Defects are almost always created, often deliberately, during manufacturing processes and further evolve in service. During the operation of a nuclear reactor, the atoms in structural components are repeatedly displaced by irradiating particles, injecting large populations of defects into the matrix. This produces localised internal, 'residual', stresses that may be detrimental to material performance. Accurate characterisation methods are required to identify defect populations and subsequently control them.

A defect in a crystalline material alters the otherwise regular and periodic arrangement of atoms. The change in atomic coordination produces long-range elastic strain fields; that is, atoms far away from the defect are displaced from their lattice sites. For a point defect, the displacement field decays as the inverse square distance from the defect centre [1,2]. By measuring strains one may be able to infer the underlying distribution of defects that produce them. Various methods exist for evaluating defect concentrations from strain measurements. Simmons and Balluffi [3–6] pioneered techniques for determining the concentration of vacancies in quenched metals by comparing dimensional and lattice parameter changes in a sample.

Recently, high spatial resolution techniques such as 4D Scanning Transmission Electron Microscopy (4D-STEM) have been able to detect strain variations at nanometer length scales. Mills et al. [7] produced detailed maps of local changes in lattice parameter in heated Au and irradiated Al. Inspired by the method of Simmons and Balluffi, local vacancy concentrations in Au were determined from changes in dimensions of selected regions and variations of the local lattice parameter. For the irradiated Al samples, local compressive and tensile strains were correlated with an excess of either interstitial or vacancy type point defects.

The general problem of inferring defect concentrations from a given dataset of strain measurements is complex [8,9]. On the one hand, it is relatively straightforward to predict the strains produced by a known distribution of defects by, for example, molecular dynamics simulations or finite element methods. However, different distributions and species of defects can produce the same strain field, making the inverse problem non-trivial. Korsunsky et al. developed an 'eigenstrain reconstruction method' that, given a set of residual stress measurements, can produce a map of the stress state throughout an entire component [10,11]. The method involved inferring the full distribution of permanent strains produced by defects from residual stresses *via* a least squares optimization procedure, in effect yielding a solution for the inverse problem, although the link between the observed strain and the underlying defect distribution was not explored. Below, we present a solution to the inverse problem for an ensemble of point defects such as vacancies and/or interstitials, determining the spatially varying defect population from the field of measured strains.

* Corresponding author.
E-mail address: Andrew.Warwick@ukaea.uk (A.R. Warwick).

https://doi.org/10.1016/j.scriptamat.2024.116276
Received 18 April 2024; Received in revised form 5 July 2024; Accepted 15 July 2024
Available online 29 July 2024

Long range elastic fields are produced by lattice defects through structural relaxation. In tungsten, a single vacancy reduces the volume of a stress free material by ∼ 30% of an atomic volume Ω_{at} and a ⟨111⟩ dumbbell produces both the overall swelling of $1.7\Omega_{at}$ and shear deformation [12,13]. A distribution of defects produces in general *tensorial* misfitting strains. This may be characterised by a field of relaxation volume tensors $\omega_{ij}(\mathbf{x})$, a symmetric second rank tensor that varies with position $\mathbf{x}$ over the material volume [14], which is the same as the field of eigenstrain [15,16].

Elastic strain $e_{ij}(\mathbf{x})$ is related to a stress tensor field by Hooke's law $\sigma_{ij}(\mathbf{x}) = C_{ijkl}e_{kl}(\mathbf{x})$ for elastic constants C_{ijkl}. In mechanical equilibrium, the stress field is divergence-free [17]. The *total* strain field, which is the superposition of elastic strain and the field of relaxation volume density tensor

$$\varepsilon_{ij}(\mathbf{x}) = e_{ij}(\mathbf{x}) + \omega_{ij}(\mathbf{x}), \tag{1}$$

equals the symmetrized derivative of displacements $u_i(\mathbf{x})$ [2]. The displacements are related to $\omega_{ij}(\mathbf{x})$ *via* [16]

$$C_{ijkl}u_{k,lj}(\mathbf{x}) = C_{ijkl}\omega_{kl,j}(\mathbf{x}). \tag{2}$$

The inverse problem is to find a relaxation volume density tensor producing a given measured total strain profile, subject to the appropriate boundary conditions. Elastic strain fields are long ranged and thus strain may be observed where there is in fact no defect. Hence, it is not immediately obvious how to determine the spatial variation of defect populations.

For isotropic defect populations, such as vacancies [14,12,13] or even solute atoms in alloys [18], the tensor relaxation volume density is

$$\omega_{ij}(\mathbf{x}) = \frac{1}{3}\omega(\mathbf{x})\delta_{ij}, \tag{3}$$

where δ_{ij} is the Kronecker delta tensor. Function $\omega(\mathbf{x})$ is related to the vacancy concentration $c_{Vac}(\mathbf{x})$ by

$$\omega(\mathbf{x}) = c_{Vac}(\mathbf{x})\frac{\Omega_{Vac}}{\Omega_{at}}, \tag{4}$$

where Ω_{Vac} is the relaxation volume of a vacancy [19].

We seek solutions to Eq. (2) subject to periodic boundary conditions (PBC). In isotropic elasticity, the field of displacements produced directly by the source $\omega(\mathbf{x})$ satisfies

$$\nabla\cdot\mathbf{u}(\mathbf{x}) = \frac{1}{3}\frac{1+\nu}{1-\nu}\delta\omega(\mathbf{x}) + \langle\omega\rangle, \tag{5}$$

where ν is Poisson's ratio, $\langle\cdot\rangle$ denotes a volume average over the periodically translated simulation cell and the fluctuation field $\delta\omega(\mathbf{x}) := \omega(\mathbf{x}) - \langle\omega\rangle$. A derivation of Eq. (5) is given in the supplementary material S1. There is a clear analogy with the Maxwell equation [20] $\nabla\cdot\mathbf{E}(\mathbf{x}) = 4\pi\rho(\mathbf{x})$ for electric field $\mathbf{E}$ and charge density $\rho(\mathbf{x})$. Under PBC, no sensible solution exists unless the charge neutrality condition is imposed. For the elasticity problem this is equivalent to imposing the condition of vanishing average stress, or, equivalently, vanishing average elastic strain [21]. Noting that $\nabla\cdot\mathbf{u}(\mathbf{x}) = \varepsilon_{ii}(\mathbf{x})$, vanishing stress implies uniform total dilatation $\langle\varepsilon_{ii}\rangle = \langle\omega\rangle$. Furthermore, for reference temperature T, thermal eigenstrains in cubic metals adopt the isotropic form $\alpha T\delta_{ij}$ [15, §1] for thermal expansion coefficient α. At thin-film length scales, the temperature is homogeneous [22, §10.1.2] and thus the thermal lattice strain may be removed from the mean dilatation.

The solution of the inverse problem is now

$$c_{Vac}(\mathbf{x}) = \frac{\Omega_{at}}{\Omega_{Vac}}\left[3\frac{1-\nu}{1+\nu}\delta\varepsilon_{ii}(\mathbf{x}) + \langle\varepsilon_{ii}\rangle - 3\alpha T\right], \tag{6}$$

where $\delta\varepsilon_{ii}(\mathbf{x}) = \varepsilon_{ii}(\mathbf{x}) - \langle\varepsilon_{ii}\rangle$.

It is striking that, according to Eq. (6), the spatially varying strain is related to the volume density of defects *at the same point*. Furthermore, $\delta\varepsilon_{ii}(\mathbf{x})$ enters the equation with a prefactor $3(1-\nu)/(1+\nu)$, unlike the volume averaged strain $\langle\varepsilon_{ii}\rangle$ where no such prefactor appears [3]. In bcc W, the elastic properties are well approximated by isotropic elasticity and at room temperature the Poisson's ratio $\nu = 0.28$ [23] implies that the fluctuations in the observed local dilatations contribute ∼ 169% to the variation of the local defect concentration. The result is material dependent as, for example, the more elastically anisotropic fcc Au has the Voigt averaged Poisson ratio $\nu = 0.42$ at room temperature [24,25], yielding the prefactor of ∼ 122% instead.

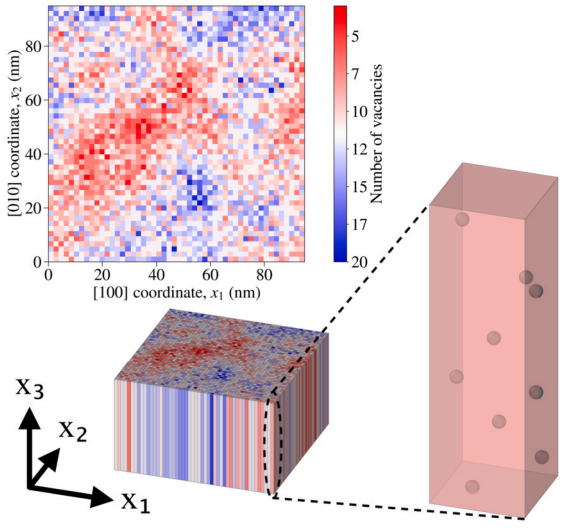

Fig. 1. Schematic of the distribution of vacancies in simulation cell. Top left is a vacancy number map with [001] pointing out of the screen. Bottom left is the corresponding simulation cell. The circled column oriented along [001] is magnified on the right, containing nine vacancies as indicated by the colour of the column and the colormap. (For interpretation of the colours in the figure(s), the reader is referred to the web version of this article.)

For the spatially homogeneously distributed vacancies [3], the role of the elastic prefactor is negligible, but for the fluctuating distributions of defects produced by irradiation [7], elasticity has a striking effect on the relation between the spatially varying strain and the spatially varying concentration of defects.

We have tested the relationship in Eq. (6) in atomistic simulations of W and Au thin films containing vacancies. The strain data extracted from simulations are compared to linear elastic finite element modelling (FEM). We employed the LAMMPS [26] program to relax 100 nm×100 nm×50 nm boxes of 32,373,068 bcc W or 36,544,848 fcc Au atoms, comparable to the dimensions of a scanned region and foil thicknesses presented by Mills et al. [7]. Interatomic forces in W and Au were modelled by the Mason et al. [27] and Sheng et al. [28] EAM potentials respectively. The lattice parameter, Voigt averaged Poisson's ratio and vacancy relaxation volume for each potential are given in the supplementary material S2. Forces were reduced to less than 10^{-4} eV/Å on any given atom and the cell shape was relaxed to zero stress conditions *via* the conjugate gradient and FIRE [29] algorithms. The simulations were run at temperature $T = 0$, removing the corresponding uniform field in Eq. (6) from the following analyses. This simplification does not affect the validity of the analysis so long as the temperature is low enough that vacancies are immobile on the timescale of interest. The elastic fields given by the same vacancy distributions were calculated by FEM, using the ABAQUS software, on a mesh of 50,000 hexahedral elements. The materials were assigned anisotropic stiffness tensors. PBC were enforced by assigning identical displacements on nodes that were periodic images of one another.

Thin-foil measurements of strain *via* 4D-STEM produce depth-averaged values. Therefore, two-dimensional (2D) concentration profiles of vacancies were generated for the atomistic simulations, as shown in Fig. 1. The x_1-x_2 face of a given simulation cell was partitioned into an evenly spaced grid of columns and, for a given vacancy con-

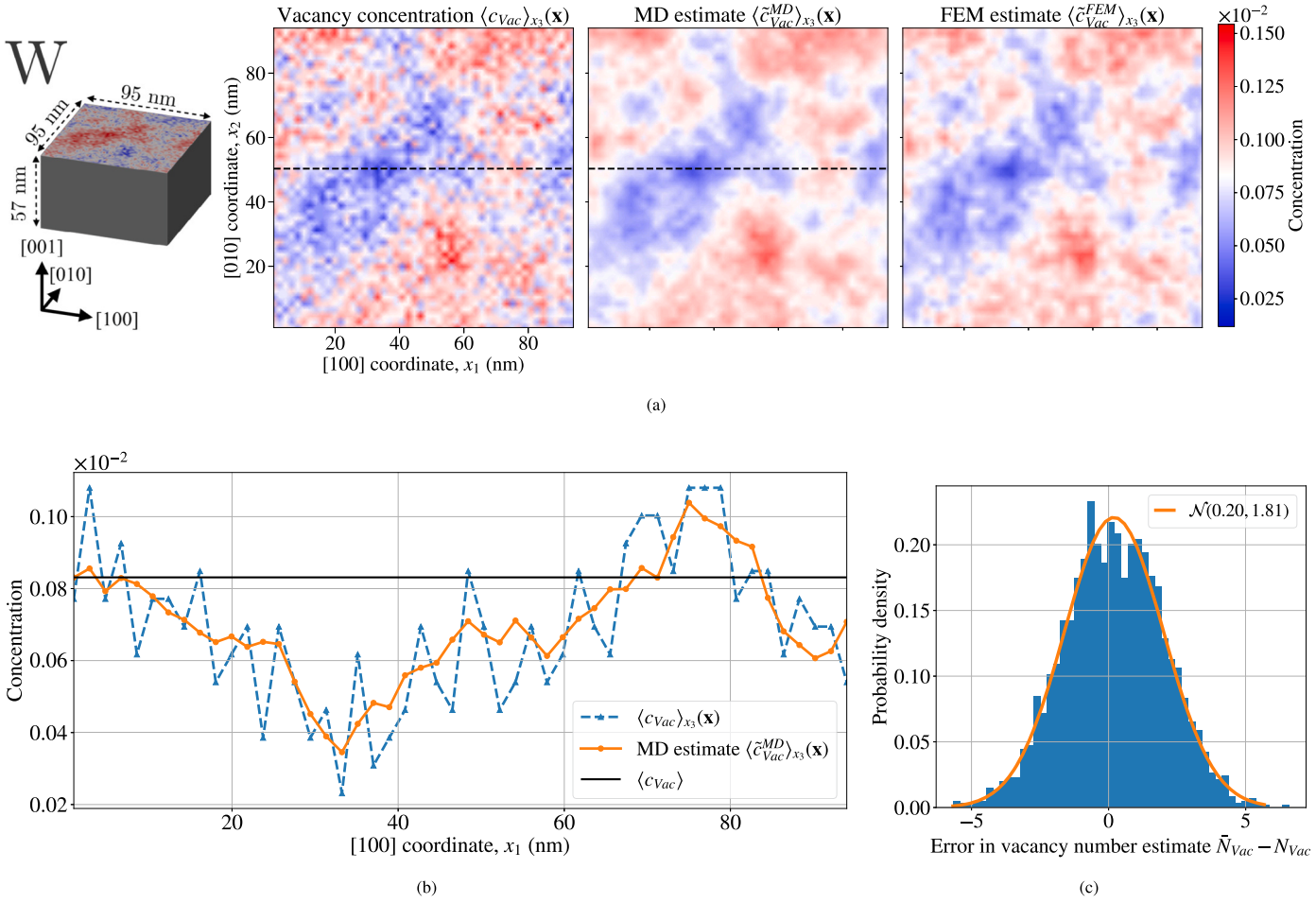

Fig. 2. (a) Left heatmap: x_3 ([001]) averaged vacancy concentration field $\langle c_{Vac}\rangle_{x_3}(\mathbf{x})$. Middle heatmap: an estimate from atomistic total dilatations for average vacancy concentration $\langle \tilde{c}^{MD}_{Vac}\rangle_{x_3}(\mathbf{x})$ according to Eq. (6). $\langle c_{Vac}\rangle_{x_3}(\mathbf{x})$ was drawn from a Gaussian random field with mean vacancy concentration $\langle c_{Vac}\rangle = 0.1\%$ and exponential correlation function given by Eq. (7) with standard deviation $\sigma_{c_{Vac}} = 0.02\%$ and correlation length $l = 20$ nm. Right heatmap: vacancy concentration based on finite element dilatation, $\langle \tilde{c}^{FEM}_{Vac}\rangle_{x_3}(\mathbf{x})$, is shown for validation. (b) Line plot along the dashed path in (a) comparing true and atomistic estimated vacancy concentrations. (c) Inverting $\langle \tilde{c}^{MD}_{Vac}\rangle_{x_3}(\mathbf{x})$ into vacancy number shows that $\langle \tilde{c}^{MD}_{Vac}\rangle_{x_3}(\mathbf{x})$ fluctuates about the linear elastic result, enabling the number of vacancies to be predicted with a standard deviation of ~ 2 vacancies.

centration profile, a corresponding number of atoms in a column were randomly removed. Values for $c_{Vac}(\mathbf{x})$ were drawn from a homogeneous and isotropic Gaussian random field with an exponential covariance function

$$C(r) = \sigma^2_{c_{Vac}} e^{-r/l}, \tag{7}$$

where $\sigma_{c_{Vac}}$ is the standard deviation and the correlation length l controls the distance over which two points separated by distance r in the random field are significantly correlated [30]. For both W and Au, the random field was parameterised by $\langle c_{Vac}\rangle = 0.1\%$, $\sigma_{c_{Vac}} = \langle c_{Vac}\rangle/5$. A correlation length of $l = 20$ nm was chosen for W and correlation lengths of 10 nm and 68 nm are presented for Au. Vacancies were distributed amongst columns with ~ 3 nm^2 cross sectional area to allow for smoothly varying concentration profiles: consider that for a column of atoms with 1 nm^2 cross sectional area in a 50 nm thick foil, similar to a single pixel in the heatmaps presented in [7], the local concentration of a single vacancy is already on the order of 0.1%. The random fields were generated by the Python package GSTools version 1.5.1 [31].

There are multiple valid definitions of strain at atomic length scale. Here, displacements of every atom from initial to relaxed configurations were voxelized, and then derivatives were computed *via* central differences. The strains were subsequently averaged along [001]. In the FEM simulations, for a given node of the hexahedral mesh with volume V_{Node}, the number of vacancies nearest to that node was computed and subsequently assigned a relaxation volume density according to Eq. (4).

The [001] averaged relaxation volume density and total dilatations for a random field of vacancies in bcc W are shown in Fig. 2. The x_1, x_2 and x_3 directions are parallel to [100], [010] and [001] respectively. Estimations $\langle \tilde{c}^{MD}_{Vac}\rangle_{x_3}(\mathbf{x})$ and $\langle \tilde{c}^{FEM}_{Vac}\rangle_{x_3}(\mathbf{x})$ of the x_3-averaged vacancy concentration $\langle c_{Vac}\rangle_{x_3}(\mathbf{x})$ were computed from atomistic and FEM total dilatations respectively *via* Eq. (6). In Fig. 2a the heatmaps of the vacancy concentration in W together with the atomistic and FEM estimates of $c_{Vac}(\mathbf{x})$ demonstrate the accuracy of applying Eq. (6) for the extraction of vacancy concentrations. A line plot of $\langle c_{Vac}\rangle_{x_3}(\mathbf{x})$ and $\langle \tilde{c}^{MD}_{Vac}\rangle_{x_3}(\mathbf{x})$ is shown in Fig. 2b. The FEM simulation confirms the linear elastic relationship described by Eq. (6), with small differences arising from the slight deviation of W from isotropic elasticity.

Eq. (6) also enables estimating the number of vacancies $\bar{N}_{Vac}$ in a column. The density plot of the absolute error $\bar{N}_{Vac} - N_{Vac}$ in Fig. 2 follows a normal distribution $\mathcal{N}(\mu, s)$ for mean $\mu \sim 0$ and standard deviation $s \sim 2$. The distribution suggests that the number of vacancies can be accurately estimated within a standard deviation of ~ 2 vacancies; even at spatial resolutions on the order of a lattice parameter, the local vacancy population can be calculated with reasonable accuracy. The role of vacancy clustering was assessed by relaxing boxes of 11,664 atoms containing different concentrations of uniformly distributed va-

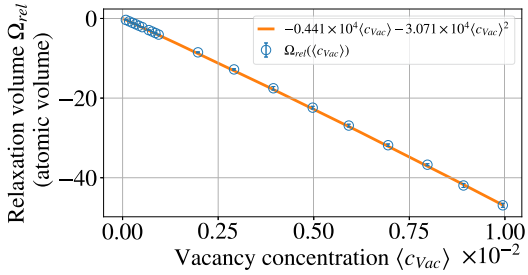

Fig. 3. Relaxation volume of a box of 11,664 W atoms containing different concentrations of uniformly distributed vacancies. Each vacancy concentration was drawn and relaxed ten times with the average and standard deviation of resulting relaxation volume Ω_{rel} plotted. The orange curve is a least squares fit according to the quadratic given in Eq. (8).

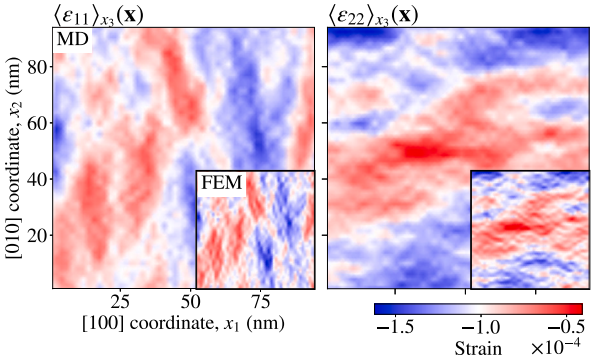

Fig. 4. Atomistic (denoted 'MD') x_3-averaged total strain components $\langle\varepsilon_{11}\rangle_{x_3}(\mathbf{x})$ (left) and $\langle\varepsilon_{22}\rangle_{x_3}(\mathbf{x})$ (right) for the random field vacancy distribution in bcc W presented in Fig. 2. Corresponding FEM strain components are shown in the inset.

cancies. The overall relaxation volume of the boxes Ω_{rel} as a function of vacancy concentration is expected to follow

$$\Omega_{rel}(\langle c_{Vac}\rangle) = k_1\langle c_{Vac}\rangle + k_2\langle c_{Vac}\rangle^2, \tag{8}$$

where the coefficients k_1 and k_2 arise from monovacancy and divacancy contributions. Fig. 3 shows the variation of Ω_{rel} with $\langle c_{Vac}\rangle$. The average of Ω_{rel} over all ten runs is plotted with error bars indicating the standard deviation. Eq. (8) was fitted *via* a least squares procedure with the values of k_1 and k_2 given in the plot. The fitted coefficients indicate that at $\langle c_{Vac}\rangle = 0.1\%$ the quadratic term is a non-negligible 1% of the linear term.

It should be emphasized that only the total dilatation, and not individual components of lattice strain, is strongly correlated with the local vacancy concentration. Therefore, if dilatation is measured by relative changes in the lattice parameter then it is important to average such lattice strains over all directions *e.g.* by averaging {100} peak shifts in a diffraction pattern. Indeed, as predicted by the anisotropic correlation functions derived by Geslin et al. [32], the x_3-averaged atomistic strain components $\langle\varepsilon_{11}\rangle_{x_3}(\mathbf{x})$ and $\langle\varepsilon_{22}\rangle_{x_3}(\mathbf{x})$ plotted in Fig. 4 present significant qualitative differences to $\langle c_{Vac}\rangle_{x_3}(\mathbf{x})$ with FEM simulations also shown for validation. Qualitatively similar profiles of strain components have been observed in thin films of irradiated W [33] and high entropy alloys where fluctuations in coordination of the alloying elements provide centres of isotropic expansion or contraction to a good approximation [34].

Applying Eq. (6) to relaxed random fields of vacancies of different correlation lengths in the elastically anisotropic fcc Au, as shown in Fig. 5, we find that the Voigt average Poisson's ratio $\nu = 0.42$ gives a good fit. Despite the high anisotropy ratio of the elastic constants, the local volume changes are strongly correlated with the underlying relaxation volume density. The effective Poisson ratio for gold

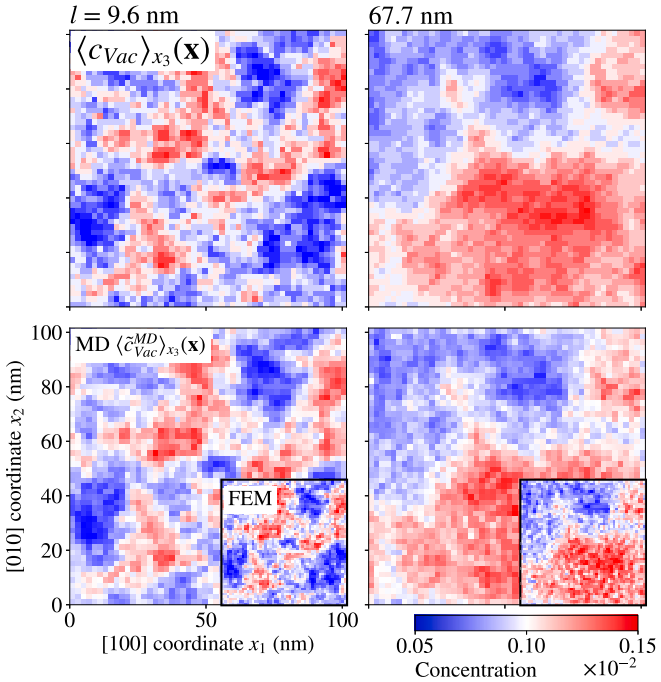

Fig. 5. x_3 ([001]) averaged vacancy concentration (top row) in Au with the corresponding x_3 averaged estimate of vacancy concentration from atomistic dilatation (bottom row) as computed by MD $\langle\tilde{c}^{MD}_{Vac}\rangle_{x_3}(\mathbf{x})$. Insets in the bottom row show the FEM estimates $\langle\tilde{c}^{FEM}_{Vac}\rangle_{x_3}(\mathbf{x})$. Mean concentration $\langle c_{Vac}\rangle = 0.1\%$ and standard deviation $\sigma_{c_{Vac}} = 0.02\%$. Across different correlation lengths l for the correlation function in Eq. (7), increasing from left to right, we observe that Eq. (6) remains a good approximation to the inverse problem.

renders the prefactor $3(1-\nu)/(1+\nu)$ close to unity. The anisotropic FEM results indicate that, throughout all the x_3 averaged concentration maps of different correlation lengths in Fig. 5, the absolute error $\left|\langle\tilde{c}^{FEM}_{Vac}\rangle_{x_3}(\mathbf{x}) - \langle c_{Vac}\rangle_{x_3}(\mathbf{x})\right|$ is on average $8\cdot10^{-3}\%$ and attains a maximum of $2\cdot10^{-2}\%$. Since the concentration of a single vacancy in a column is $7\cdot10^{-3}\%$, the mean absolute error from applying Eq. (6) is equivalent to 1 vacancy and is off by at most 2 vacancies.

A thin foil suspended in an electron microscope does not have periodic boundaries. We may model a foil as periodic in x_1 and x_2 but with a traction free surface perpendicular to x_3. The mean stress theorem states that in a traction free body the volume average of stress $\langle\sigma_{ij}\rangle$ vanishes [17, §15.1]. It follows that the elastic strain vanishes and therefore according to Eq. (1) the average strain of the body $\langle\varepsilon_{ij}\rangle = \langle\omega_{ij}\rangle$. In earlier work, we showed that the dilatation in a traction free thin film is well approximated by Eq. (6) [16]. Deviations from this result stem from image strains arising from the free surface. In regions sufficiently far away from the surface, the strain fields are well described by Eq. (6). For example, the bulk of W neutron-irradiated at 800° was found to contain a large concentration of voids except near grain boundaries in denuded zones approximately 30 nm thick [35]; such zones will be thinner at lower temperatures. Indeed, we find that the distribution of absolute errors in vacancy number was not significantly altered after relaxing, *i.e.* effectively at temperatures below the corresponding vacancy migration energy, the random field of vacancies in W with a free (001) surface may still be inferred *via* Eq. (6) with reasonable accuracy.

We may extend the preceding analysis to isotropic eigenstrains that are not comprised solely of vacancies. For some materials that contain mostly isotropic eigenstrain, it is still possible to extract the vacancy distribution. As previously discussed, thermal strains can be readily corrected for. Furthermore, strains arising from solutes may be accounted for *via* techniques such as electron energy loss spectroscopy (EELS) that determine the location and concentration of impurity elements [35]. With reference to relaxation volume data of solutes in the given host

lattice, *e.g.* [36], one may correct for their contribution to the local total dilatation.

Metals that are lightly irradiated to doses $\ll 0.1$ dpa, and have initially low concentrations of defects, develop a combination of small self interstitial atom (SIA) clusters and vacancies that produce isotropic eigenstrain. For example, SIAs in fcc Al coalesce into A15 clusters whose eigenstrain is purely dilatational [37]. However $\varepsilon_{ii}(\mathbf{x})$ is now proportional to the sum of SIA cluster and vacancy relaxation volume densities, rendering the inverse problem underdetermined and it is thus unlikely that concentrations of each type of defect can be known precisely. Regardless, the relaxation volume density $\omega(\mathbf{x})$ in Eq. (5) can always be extracted in such systems, providing a measure of the magnitude of compression or tension enforced by the underlying defects on the surrounding lattice. Furthermore, by solving for the elastic strain with Eqs. (1) and (5) it is straightforward to estimate the local stress state.

CRediT authorship contribution statement

Andrew R. Warwick: Writing – review & editing, Writing – original draft, Visualization, Methodology, Formal analysis, Data curation. **Luca Reali:** Writing – review & editing, Visualization, Methodology, Formal analysis, Data curation. **Sergei L. Dudarev:** Writing – review & editing, Supervision, Resources, Funding acquisition, Formal analysis, Conceptualization.

Declaration of competing interest

The authors declare that they have no known competing financial interests or personal relationships that could have appeared to influence the work reported in this paper.

Acknowledgements

This work has been carried out within the framework of the EUROfusion Consortium, funded by the European Union via the Euratom Research and Training Programme (Grant Agreement No 101052200-EUROfusion) and the Broader Approach Activity Phase II under the Procurement Agreement IFERC2-T2PA02. This work was also funded by the EPSRC Energy Programme (Grant Number EP/W006839/1). To obtain further information on the data and models underlying the paper please contact PublicationsManager@ukaea.uk. Views and opinions expressed are however those of the authors only and do not necessarily reflect those of the European Union or the European Commission. Neither the European Union nor the European Commission can be held responsible for them. This study was performed using the resources provided by the Cambridge Service for Data Driven Discovery (CSD3).

Appendix. Supplementary material

Supplementary material related to this article can be found online at https://doi.org/10.1016/j.scriptamat.2024.116276.

References

[1] A.M. Kosevich, The Crystal Lattice, Wiley-VCH, Weinheim, 2005.
[2] A.P. Sutton, Physics of Elasticity and Crystal Defects, Oxford University Press, 2020.
[3] R.O. Simmons, R.W. Balluffi, Measurements of equilibrium vacancy concentrations in aluminum, Phys. Rev. 117 (1) (1960) 52–61, https://doi.org/10.1103/PhysRev.117.52.
[4] R.O. Simmons, R.W. Balluffi, Measurement of the equilibrium concentration of lattice vacancies in silver near the melting point, Phys. Rev. 119 (2) (1960) 600–605, https://doi.org/10.1103/PhysRev.119.600.
[5] R.O. Simmons, R.W. Balluffi, Measurement of equilibrium concentrations of lattice vacancies in gold, Phys. Rev. 125 (3) (1962) 862–872, https://doi.org/10.1103/PhysRev.125.862.
[6] R.O. Simmons, R.W. Balluffi, Measurement of equilibrium concentrations of vacancies in copper, Phys. Rev. 129 (4) (1963) 1533–1544, https://doi.org/10.1103/PhysRev.129.1533.
[7] S.H. Mills, S.E. Zeltmann, P. Ercius, A.A. Kohnert, B.P. Uberuaga, A.M. Minor, Nanoscale mapping of point defect concentrations with 4D-STEM, Acta Mater. 246 (2023) 118721, https://doi.org/10.1016/j.actamat.2023.118721.
[8] F. Hofmann, E. Tarleton, R.J. Harder, N.W. Phillips, P.-W. Ma, J.N. Clark, I.K. Robinson, B. Abbey, W. Liu, C.E. Beck, 3D lattice distortions and defect structures in ion-implanted nano-crystals, Sci. Rep. 7 (2017) 45993, https://doi.org/10.1038/srep45993.
[9] S. Hu, Q. Li, H. Sun, X. Lv, M. Song, Y. Zhao, R. Zhang, C. Zhang, Y. Shen, Y. Liu, T. Fan, Introducing vacancy defects by rapid quenching in FCC metal for deep learning micrograph dataset, Mater. Charact. (2024) 113827, https://doi.org/10.1016/j.matchar.2024.113827.
[10] A.M. Korsunsky, K.E. Wells, P.J. Withers, Mapping two-dimensional state of strain using synchroton X-ray diffraction, Scr. Mater. 39 (12) (1998) 1705–1712, https://doi.org/10.1016/S1359-6462(98)00385-6.
[11] T.-S. Jun, A.M. Korsunsky, Evaluation of residual stresses and strains using the eigenstrain reconstruction method, Int. J. Solids Struct. 47 (13) (2010) 1678–1686, https://doi.org/10.1016/j.ijsolstr.2010.03.002.
[12] P.-W. Ma, S.L. Dudarev, Universality of point defect structure in body-centered cubic metals, Phys. Rev. Mater. 3 (2019) 013605, https://doi.org/10.1103/PhysRevMaterials.3.013605.
[13] P.-W. Ma, S.L. Dudarev, Nonuniversal structure of point defects in face-centered cubic metals, Phys. Rev. Mater. 5 (2021) 013601, https://doi.org/10.1103/PhysRevMaterials.5.013601.
[14] S.L. Dudarev, D.R. Mason, E. Tarleton, P.-W. Ma, A.E. Sand, A multi-scale model for stresses, strains and swelling of reactor components under irradiation, Nucl. Fusion 58 (2018) 126002, https://doi.org/10.1088/1741-4326/aadb48.
[15] T. Mura, Micromechanics of Defects in Solids, 2nd edition, Kluwer Academic Publishers, Dordrecht, the Netherlands, 1991.
[16] L. Reali, M. Boleininger, M.R. Gilbert, S.L. Dudarev, Macroscopic elastic stress and strain produced by irradiation, Nucl. Fusion 62 (1) (2022) 016002, https://doi.org/10.1088/1741-4326/ac35d4.
[17] C. Teodosiu, Elastic Models of Crystal Defects, Springer Berlin Heidelberg, Berlin, Heidelberg, 1982.
[18] B. Sboui, D. Rodney, P.-A. Geslin, Elastic modelling of lattice distortions in concentrated random alloys, Acta Mater. 257 (2023) 119117, https://doi.org/10.1016/j.actamat.2023.119117.
[19] P.-W. Ma, S.L. Dudarev, Effect of stress on vacancy formation and migration in body-centered-cubic metals, Phys. Rev. Mater. 3 (2019) 063601, https://doi.org/10.1103/PhysRevMaterials.3.063601.
[20] L.D. Landau, E.M. Lifshitz, The Classical Theory of Fields, Pergamon Press, Oxford, 1971.
[21] S.L. Dudarev, P.-W. Ma, Elastic fields, dipole tensors, and interaction between self-interstitial atom defects in bcc transition metals, Phys. Rev. Mater. 2 (2018) 033602, https://doi.org/10.1103/PhysRevMaterials.2.033602.
[22] L. Reimer, Transmission Electron Microscopy: Physics of Image Formation and Microanalysis, Springer Series in Optical Sciences, vol. 36, Springer, Berlin, Heidelberg, 1997.
[23] F.H. Featherston, J.R. Neighbours, Elastic constants of tantalum, tungsten, and molybdenum, Phys. Rev. 130 (1963) 1324–1333, https://doi.org/10.1103/PhysRev.130.1324.
[24] W. Voigt, Lehrbuch der Kristallphysik, Vieweg+Teubner Verlag, Wiesbaden, 1966.
[25] J.R. Neighbours, G.A. Alers, Elastic constants of silver and gold, Phys. Rev. 111 (3) (1958) 707–712, https://doi.org/10.1103/PhysRev.111.707.
[26] A.P. Thompson, H.M. Aktulga, R. Berger, D.S. Bolintineanu, W.M. Brown, P.S. Crozier, P.J. in 't Veld, A. Kohlmeyer, S.G. Moore, T.D. Nguyen, R. Shan, M.J. Stevens, J. Tranchida, C. Trott, S.J. Plimpton, LAMMPS - a flexible simulation tool for particle-based materials modeling at the atomic, meso, and continuum scales, Comput. Phys. Commun. 271 (2022) 108171, https://doi.org/10.1016/j.cpc.2021.108171.
[27] D.R. Mason, D. Nguyen-Manh, C.S. Becquart, An empirical potential for simulating vacancy clusters in tungsten, J. Phys. Condens. Matter 29 (50) (2017) 505501, https://doi.org/10.1088/1361-648X/aa9776.
[28] H.W. Sheng, M.J. Kramer, A. Cadien, T. Fujita, M.W. Chen, Highly optimized embedded-atom-method potentials for fourteen fcc metals, Phys. Rev. B 83 (13) (2011) 134118, https://doi.org/10.1103/PhysRevB.83.134118.
[29] E. Bitzek, P. Koskinen, F. Gähler, M. Moseler, P. Gumbsch, Structural relaxation made simple, Phys. Rev. Lett. 97 (17) (2006) 170201, https://doi.org/10.1103/PhysRevLett.97.170201.
[30] R. Webster, M.A. Oliver, Modelling the Variogram, John Wiley & Sons, Ltd, 2007, pp. 77–107, Ch. 5.
[31] S. Müller, L. Schüler, A. Zech, F. Heße, GSTools v1.3: a toolbox for geostatistical modelling in python, Geosci. Model Dev. 15 (7) (2022) 3161–3182, https://doi.org/10.5194/gmd-15-3161-2022.
[32] P.-A. Geslin, A. Rida, D. Rodney, Microelasticity model of random alloys. Part II: displacement and stress correlations, J. Mech. Phys. Solids 153 (2021) 104480, https://doi.org/10.1016/j.jmps.2021.104480.
[33] G. He, H. Yu, P. Karamched, J. Liu, F. Hofmann, Elastic strain associated with irradiation-induced defects in self-ion irradiated tungsten, Scr. Mater. 237 (2023) 115687, https://doi.org/10.1016/j.scriptamat.2023.115687.
[34] Q. Ding, Y. Zhang, X. Chen, X. Fu, D. Chen, S. Chen, L. Gu, F. Wei, H. Bei, Y. Gao, M. Wen, J. Li, Z. Zhang, T. Zhu, R.O. Ritchie, Q. Yu, Tuning element distribution,

structure and properties by composition in high-entropy alloys, Nature 574 (7777) (2019) 223–227, https://doi.org/10.1038/s41586-019-1617-1.

[35] M. Dürrschnabel, M. Klimenkov, U. Jäntsch, M. Rieth, H.C. Schneider, D. Terentyev, New insights into microstructure of neutron-irradiated tungsten, Sci. Rep. 11 (1) (2021) 7572, https://doi.org/10.1038/s41598-021-86746-6.

[36] L. Gharaee, P. Erhart, A first-principles investigation of interstitial defects in dilute tungsten alloys, J. Nucl. Mater. 467 (2015) 448–456, https://doi.org/10.1016/j.jnucmat.2015.09.003.

[37] T. Jourdan, A. Goryaeva, M.-C. Marinica, Preferential nucleation of dislocation loops under stress explained by A15 Frank-Kasper nanophases in aluminum, Phys. Rev. Lett. 132 (22) (2024) 226101, https://doi.org/10.1103/PhysRevLett.132.226101.